ORIGINAL ARTICLE

Oceanic dispersion simulation of perfluoroalkyl substances in the Western North Pacific associated with the Great East Japan Earthquake of 2011

Yasumasa Miyazawa · Nobuyoshi Yamashita ·
Sachi Taniyasu · Eriko Yamazaki · Xinyu Guo ·
Sergey M. Varlamov · Toru Miyama

Abstract The Great East Japan Earthquake on 11 March 2011, followed by the tsunami and fire, resulted in serious environmental problems in and around Japan. A huge amount of material was discharged into the ocean after the tremendous flood damage of the tsunami. A monitoring survey of the perfluoroalkyl substances (PFAs) found evidence showing an abrupt increase in the PFA concentration in the ocean east of Japan in 2011 after the earthquake. To confirm the anomalous input of two typical PFAs, perfluorooctanoate (PFOA) and perfluorooctanesulfonate (PFOS), from the Japanese coast into the ocean, associated with the earthquake, we conducted a series of chemical tracer simulations using an eddy-resolving ocean reanalysis product: JCOPE2. The simulation model involves processes representing the emission of PFAs from the land triggered by the tsunami flood, advection of the polluted waters, and decay of the concentration by the background oceanic turbulence. Comparison of the PFOA simulation results with the observation confirms a spike-like input of PFOA into the Western North Pacific after the earthquake. Advection and diffusion by the Kuroshio Extension and the mesoscale eddies play a key role in the dilution of the concentration. Optimization of unknown simulation parameters leads to an estimation of the total amount of the anomalous PFOA emission. In contrast, the PFOS simulations are not able to explain the observed distribution, suggesting possible differences in the oceanic transport processes between PFOS and PFOA.

1 Introduction

Oceanic distribution of perfluoroalkyl substances (PFAs) including perfluorooctanoate (PFOA) and perfluorooctanesulfonate (PFOS) has been investigated (Yamashita et al. 2004) since the first discovery of the accumulation of PFOS in a number of marine wildlife animals (Giesy and Kannan 2001). PFAs have been manufactured for over 60 years and are widely spread throughout the environment. An international collaborative study for the global ocean monitoring of PFAs has been carried out since 2002 by the National Institute of Advanced Industrial Science and Technology in Japan, the Ocean Research Institute of the University of Tokyo, and the Leibniz Institute of Marine Sciences in Germany (Yamashita et al. 2005). PFAs are important not only for risk assessment in the environment, but also for effective tracing of the general circulation of the oceans on the global and regional scale (Yamashita et al. 2008).

The international PFA monitoring group recently found that the subsurface concentration of PFA at sampling points east of Japan was much higher in July 2011 after the Great East Japan Earthquake on 11 March 2011 (EQ 3.11) than that observed in June 2010 prior to EQ 3.11

Y. Miyazawa (✉) · X. Guo · S. M. Varlamov · T. Miyama
Japan Agency for Marine-Earth Science and Technology,
3173-25 Showa-machi, Kanazawa-ku,
Yokohama 236-0001, Japan
e-mail: miyazawa@jamstec.go.jp

N. Yamashita · S. Taniyasu · E. Yamazaki
National Institute of Advanced Industrial Science and
Technology, Tsukuba, Ibaraki 305-8569, Japan

X. Guo
Ehime University, Matsuyama, Ehime 790-8577, Japan

Fig. 1 Vertical profiles of the observed PFOA and PFOS concentration. **a** Measurement at 144.505°E, 40.466°N on 22 June 2010. **b** As in **a** except for the zoom-up view in the upper 1,100-m layer. **c** Measurement 143.873°E, 37.866°N on 31 July 2011. **d** As in **c** except for zoom-up view in upper 1,100-m layer
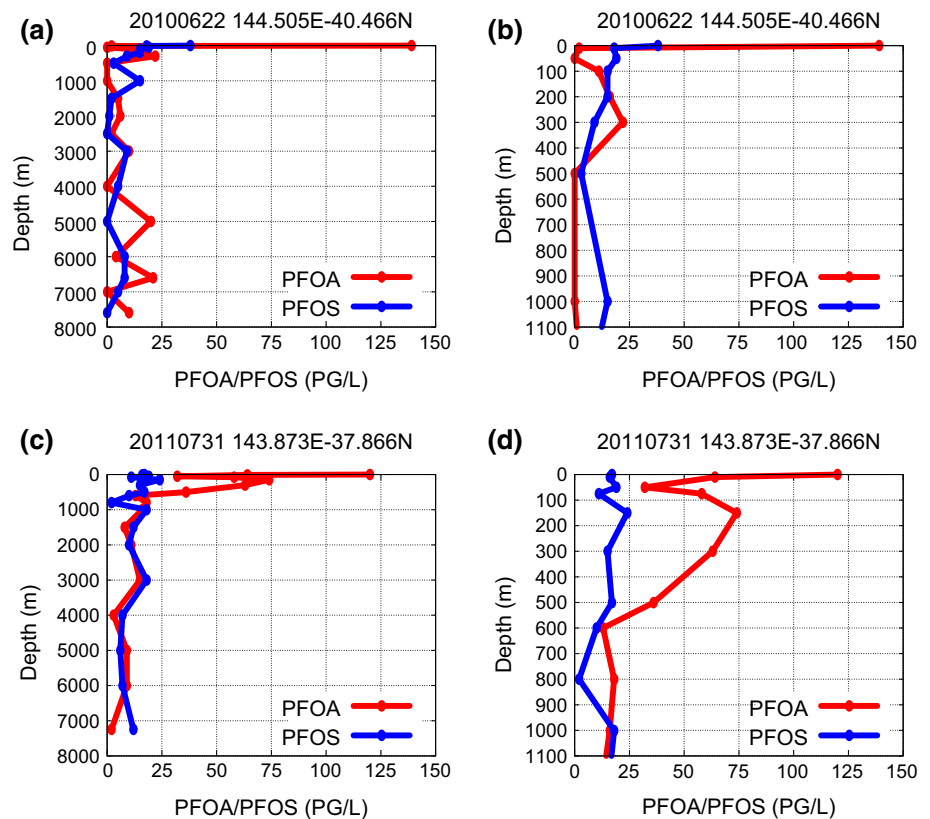
(Yamazaki et al. 2012). The PFOA and PFOS profiles obtained east of Japan by a research cruise of the R/V Hakuho Maru (KH-10-02) in June 2010 before EQ 3.11 (Fig. 1a, b) indicate the maximum concentration at the surface together with a few local maxima at deep levels, implying possible effects of the airborne PFAs near the surface and re-distribution in the deep layer caused by the dense bottom water around the slope of the Japan Trench (Yamazaki et al. 2012). The maximum concentration values in the subsurface levels of the profiles obtained before EQ 3.11 are around 20 pg/l. The profiles obtained by a cruise of the same R/V (KH-11-07) after EQ 3.11 exhibit a significant increase in the concentration in the upper 1,000-m-depth layer (Fig. 1c, d), even though the surface concentrations of the profiles obtained before EQ 3.11 were higher than those obtained after EQ 3.11.

The tremendous flood associated with the tsunami triggered by EQ 3.11 resulted in a huge amount of marine debris floating over a wide range of the North Pacific (Showstack 2011). Various kinds of chemical compounds including PFAs together with the debris could have been discharged into ocean from the east coast of Japan after EQ 3.11; however, so far no studies have focused on numerical simulations of these phenomena. This study aims at numerically simulating the oceanic dispersion of PFAs discharged into the ocean triggered by EQ 3.11.

It is well known that a huge amount of radionuclides originating from the Fukushima Daiichi Nuclear Power Plant was discharged into the Western North Pacific after EQ 3.11, and the ocean forecast and reanalysis using numerical models have been intensively utilized for tracking of the oceanic dispersion of the radionuclides (e.g., Masumoto et al. 2012; Miyazawa et al. 2012, 2013). Estimation of the source information including the total emission amounts of the radionuclides into the environment has been a central issue for the investigation of the radionuclide dispersion (e.g., Miyazawa et al. 2013). We utilized the JCOPE2 ocean reanalysis (Miyazawa et al. 2009) for simulation of the oceanic dispersion of PFAs associated with EQ 3.11 and estimated the unknown simulation parameters including the source information of PFAs by adopting the same method, based on Green's function approach, as used for the previous study of oceanic radionuclide dispersion (Miyazawa et al. 2013).

This article is organized as follows. Section 2 describes the transport model of PFAs, observation data, and optimization of simulation parameters using the Green's function approach. Section 3 shows the simulation results and discusses the estimation of the simulation parameters. First, we focus on the oceanic dispersion of PFOA and later discuss the validity of the simulation of PFOS. Section 4 summarizes the results and discusses related issues.

2 Model and data

Supposing that PFAs (PFOA and PFOS) are water-soluble tracers transported by ocean currents, we conducted a series of the oceanic dispersion simulations for the period from 12 March 2011 to 30 March 2012 using a transport model of PFAs similar to that used for the radionuclide simulations associated with the accident at the Fukushima Daiichi Nuclear Power Plant (Miyazawa et al. 2012, 2013). Considering that PFOA is more water-soluble and less bio-accumulative than PFOS (Nakata et al. 2006), at first, we focused on the simulation of PFOA, then discussed the simulation of PFOS. The present model includes a source flux term representing the emission of PFAs from land into the ocean caused by the tsunami flood after EQ 3.11 and involved no other source/sink term such as the half-life decay term for the radionuclides because of the chemical stability of PFAs.

Horizontal and vertical diffusion processes are modeled by harmonic operators with horizontal and vertical diffusion coefficients estimated by the Smagorinsky (1963) formula and the Mellor-Yamada-Nakanishi-Niino-Furuichi mixed layer model (Nakanishi and Niino 2009; Furuichi et al. 2012), respectively. The Smagorinsky (1963) formula represents the horizontal diffusion coefficient,

$$K_{x,y} = C_s \Delta x \Delta y \frac{1}{2} |\nabla V + (\nabla V)^T|,$$

$$\nabla V + (\nabla V)^T = \left(\left(\frac{\partial u}{\partial x}\right)^2 + \frac{1}{2}\left(\frac{\partial v}{\partial x} + \frac{\partial u}{\partial y}\right)^2 + \left(\frac{\partial v}{\partial y}\right)^2 \right)^{1/2} \quad (1)$$

where u and v denote horizontal flow; Δx (Δy) denote a grid interval in the zonal (meridional) direction; C_s is a positive constant, whose order could be 0.1 (Mellor 2004). The Smagorinsky diffusion constant C_s is considered an adjustable parameter in this study.

We examine the dispersion of PFAs in the Western North Pacific using the daily-mean ocean current data produced by the JCOPE2 ocean reanalysis, which covers a region between 10.5°–62°N and 108°–180°E with a horizontal resolution of 1/12° and 46 generalized sigma levels from the surface to the maximum depth of 6,500 m (Miyazawa et al. 2009). The transport model uses the same grid as JCOPE2. The time step of the present simulation is 5 min, and the daily-mean horizontal current data of JCOPE2 are linearly interpolated to each time step. The vertical velocity required for the vertical advection term is calculated using the continuous equation from the horizontal current data.

To represent the possible emission processes of PFAs, we assume source grids along the east coast of Japan (Fig. 2) based on the information about the tsunami flood area provided by the Geospatial Information Authority of Japan (Nakajima and Koarai 2011). The PFA emission flux with a constant value is put on the top level of the source grid during the period from 12 to 16 March 2011. We put an equal weight for each grid because a preliminary comparison between cases with equal weight and spatially different weights depending on the corresponding flood areas (see shades in Fig. 2) shows the better skill of the former case (correlation of the observation data: 0.58; a statistically significant level for 95 % significance with a sample size of 81 is 0.22) as compared to the latter case (correlation: 0.51). The spatially different weights for the source grids enhance overestimation of the concentration at some measurement points near the coast (not shown).

The total emission amount is considered an adjustable parameter. Note that the duration of the emission (5 days) could also be an adjustable parameter, but it is not independent of the total emission amount. In this study, we choose not the duration but the total emission amount as an adjustable parameter, because a preliminary simulation with a longer emission period (10 days) shows worse skill (correlation: 0.55) than the base case with the 5-day emission period (correlation: 0.58).

Since the true states of PFA initial conditions are unclear, four different types of vertical profiles are tested as possible initial conditions in the simulation experiments
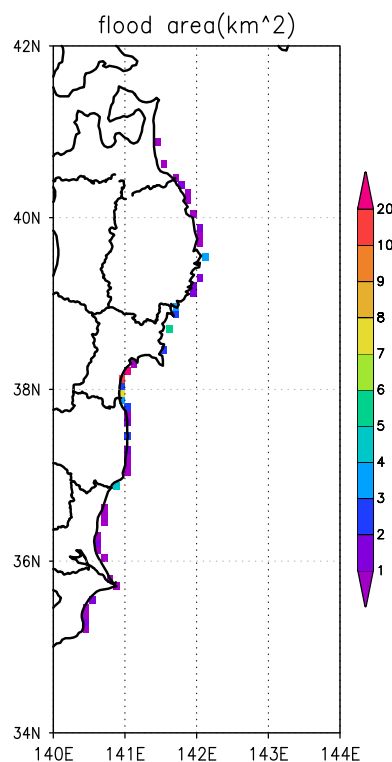

Fig. 2 Model grids near the flood-damaged regions associated with EQ 3.11. *Shaded area* indicates the flood area (in km²) in each local region estimated by the Geospatial Information Authority of Japan (Nakajima and Koarai 2011)
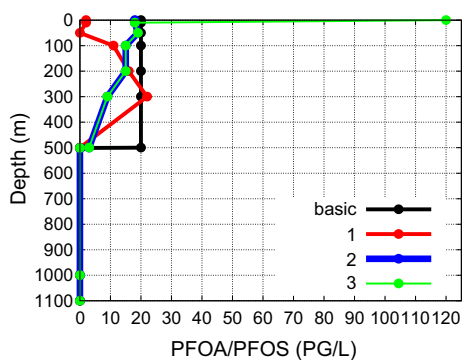
Fig. 3 Vertical profiles of the initial conditions used for the simulations

(Fig. 3). A basic case represents an initial step profile of PFAs with a constant positive value for the upper 500 m, which is an adjustable parameter, and zero below 500 m depth. Other cases are taken from the observed profiles for the upper 500 m with zero below 500 m depth. Profiles '1' and '2' are based on the observed PFOA and PFOS sub-surface profiles, respectively (Fig. 1b). To examine the effects of the relatively high concentration at the surface (Fig. 1), we test profile '3' with a surface value change from 18 to 120 pg/l for profile '2', which is similar to a typical profile found offshore around industrialized countries (Yamashita et al. 2005). The adjustable parameter for the profiles '1', '2', and '3' is a multiplication constant for the original profiles with the default value of 1.

For validation and optimization of the simulations, we utilize the data obtained by a research cruise of the R/V Hakuho Maru (KH-11-07), which sampled vertical profiles during a period from July to August 2011 (Yamazaki et al. 2012). Supposing possible contamination with airborne PFAs, we exclude the observation data at the surface (0 m) from the validation at first and then examine effects of the surface data on the validation and optimization results. Focusing on the upper ocean dispersion processes, we also exclude the data obtained at depth levels greater than 1,000 m from validation.

To adjust the parameters using the Green's function approach (Menemenlis et al. 2005; Miyazawa et al. 2013), we minimize a cost function,

$$C = \left(\vec{y} - \vec{x}^{\mathrm{f}}\right)^{\mathrm{t}} R^{-1} \left(\vec{y} - \vec{x}^{\mathrm{f}}\right) \tag{2}$$

where $\vec{x^{\mathrm{f}}} = \left(x_1^{\mathrm{f}}, \ldots x_N^{\mathrm{f}}\right)^{\mathrm{t}}$ and $\vec{y} = \left(y_1^{\mathrm{o}}, \ldots y_N^{\mathrm{o}}\right)^{\mathrm{t}}$ denote N-number concentration values of the simulation and observation, respectively; R denotes the observation error covariance matrix whose diagonal components are given by the observation errors, which are defined as 20 % of the measurement values. We ignore the error covariance between the different observation data.

Table 1 Parameters, cost, and correlation in the simulations with the initial profile 'basic'

Cases	Basic	b-P-E	b-P-I	b-P-C
Total emission amount (tons)	5.8	11.5	5.8	5.8
Initial value of the upper 500-m depth (pg/l)	20	20	40	20
Diffusion constant	0.1	0.1	0.1	0.3
Cost function value for the PFOA data	685	1,127	1,259	643
Correlation with the PFOA data	0.58	0.55	0.61	0.59
Cost function value for the PFOS data	21,565	43,269	71,422	20,508
Correlation with the PFOS data	0.15	0.11	0.21	0.16

Table 2 As in Table 1 except with the initial profile '1'

Cases	1	1-P-E	1-P-I	1-P-C
Total emission amount (tons)	5.8	11.5	5.8	5.8
Ratio to the initial profile	1	1	2	1
Diffusion constant	0.1	0.1	0.1	0.3
Cost function value for the PFOA data	1,007	1,279	991	975
Correlation with the PFOA data	0.51	0.51	0.50	0.50
Cost function value for the PFOS data	10,656	29,055	27,698	9,498
Correlation with the PFOS data	0.063	0.060	0.058	0.057

3 Results

3.1 The PFOA simulations

After performing a number of preliminary simulation experiments, we determined first guess parameter values: (1) a total emission amount for the 5-day period from 12 to 16 March 2011 as 5.76 tons, (2) an initial constant concentration value in the upper 500-m layer for the basic profile as 20 pg/l and a default multiplication constant of 1 for profiles 1–3, and (3) the Smagorinsky diffusion constant for the horizontal diffusion parameterization (1) as 0.1 (Tables 1, 2, 3, 4).

Comparison of the baseline simulation result ('basic' in Table 1) with the first guess parameters and the PFOA observation data obtained from July to August 2011 suggests a similarity between them (Fig. 4a), and the correlation value is 0.58. The Green's function approach requires results of sensitivity experiments with perturbed

Table 3 As in Table 1 except with the initial profile '2'

Cases	2	2-P-E	2-P-I	2-P-C
Total emission amount (tons)	5.8	11.5	5.8	5.8
Ratio to the initial profile	1	1	2	1
Diffusion constant	0.1	0.1	0.1	0.3
Cost function value for the PFOA data	852	1,184	727	801
Correlation with the PFOA data	0.58	0.55	0.62	0.59
Cost function value for the PFOS data	12,740	32,444	36,011	11,785
Correlation with the PFOS data	0.16	0.12	0.22	0.17

Table 4 As in Table 1 except with the initial profile '3'

Cases	3	3-P-E	3-P-I	3-P-C
Total emission amount (tons)	5.8	11.5	5.8	5.8
Ratio to the initial profile	1	1	2	1
Diffusion constant	0.1	0.1	0.1	0.3
Cost function value for the PFOA data	805	1,175	827	749
Correlation with the PFOA data	0.61	0.56	0.65	0.62
Cost function value for the PFOS data	15,018	35,502	44,941	14,099
Correlation with the PFOS data	0.20	0.14	0.27	0.21

Fig. 4 Comparison of the observed and simulated concentration of PFOA (in pg/l). **a** The baseline simulation ('basic' in Table 1). **b** The simulation with the parameters optimized for the PFOA data ('PFOA-b-s' in Table 6)

target parameters (Menemenlis et al. 2005). We conducted three sensitivity experiments required for the calculation of Green's function by perturbing each adjustable parameter in the initial profile of the basic type (Table 1). Increasing the total emission amount (b-P-E) and the initial value (b-P-I) results in larger cost function values, while increasing the Smagorinsky diffusion constant (b-P-C) leads to a cost reduction. The parameter perturbation experiments with the other initial basic profiles (Tables 2, 3, 4) show that increasing the total emission amount (1-P-E, 2-P-E, and 3-P-E) and the Smagorinsky diffusion constant (1-P-C, 2-P-C, and 3-P-C) leads to larger and smaller constant function values, respectively. The responses of the direct perturbation to the initial basic profiles seem to be more complicated: reduction (increase) of the cost function values in 1-P-I and 2-P-I (3-P-I).

As a result of the optimization through the Green's function approach accounting for the error covariance among all three parameters, the smaller emission amount, slightly larger initial concentration value, and larger Smagorinsky diffusion constant are estimated as optimal if compared to those of the baseline experiment: 'A-b-s'
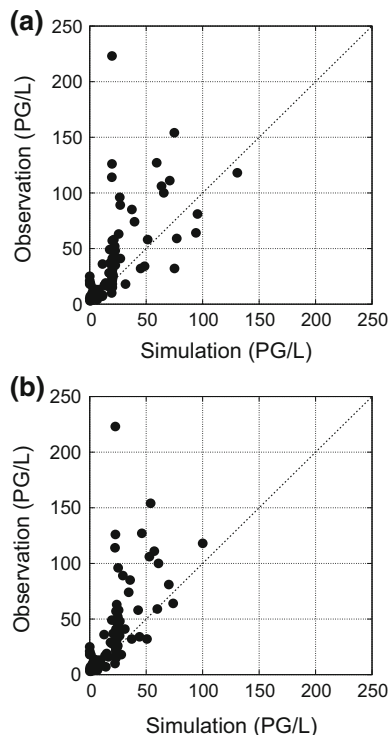
(Table 5). Use of the other initial vertical profiles results in increased values of the expected cost function with the optimized parameters 'A-1-s', 'A-2-s', and 'A-3-s', as compared to the basic case: 'A-b-s' (Table 5). The evaluated emission amounts are similar among all the cases except for 'A-1-s', which shows a larger value, 6.7 tons, than those of around 5 tons estimated for the other cases. This is considered as compensation for the low concentration in the near surface layer in the initial profile '1' (Fig. 3).

A simulation with the optimized parameters for the basic case: 'A-b-s simulation' (Table 7) shows the actual reduction of the cost function (685 → 614) similar to the expectation (618) based on the Green's function approach together with the improvement of the correlation (0.58 → 0.60), which mainly comes from the corrected overestimation owing to the decreased emission amount in the optimized case, as indicated in Fig. 4a, b. Although the correlation in the optimized case (0.60) is slightly smaller than that in the case of b-P-I (0.61), the cost function value in the former case (614) is sufficiently smaller than that in the latter case (1,127). Another simulation with the optimized parameters for the initial profile '2' represents the cost and correlation with comparable scores to the basic case ('A-2-s simulation' in Table 7) and shows the

Table 5 Optimization results with use of the PFOA observation data

Cases (expected cost)	Initial profile	Use of surface data	Emission amount ± error (tons)	Initial value ± error	Diffusion constant ± error
A-b-s (618)	Basic	No	4.8 ± 0.5	23 ± 0.8 (pg/l)	0.37 ± 0.06
A-1-s (888)	1	No	6.7 ± 0.5	1.5 ± 0.07 (multiplication constant)	0.49 ± 0.06
A-2-s (621)	2	No	5.0 ± 0.5	1.8 ± 0.06 (multiplication constant)	0.46 ± 0.06
A-3-s (629)	3	No	5.1 ± 0.5	1.5 ± 0.06 (multiplication constant)	0.48 ± 0.06
A-b-0 (1067)	Basic	Yes	1.1 ± 0.2	27 ± 0.8 (pg/l)	0.27 ± 0.03
A-1-0 (1499)	1	Yes	1.8 ± 0.2	1.8 ± 0.06 (multiplication constant)	0.32 ± 0.04
A-2-0 (1048)	2	Yes	1.0 ± 0.2	2.1 ± 0.06 (multiplication constant)	0.30 ± 0.03
A-3-0 (1048)	3	Yes	1.0 ± 0.2	1.8 ± 0.05 (multiplication constant)	0.31 ± 0.03

evolution of the oceanic dispersion generally similar to the basic case (not shown).

Figure 5 shows that the PFOA injected into the Pacific Ocean after EQ 3.11 is transported eastward by the Kuroshio Extension together with the horizontal mixing caused by the mesoscale eddies around the Kuroshio-Oyashio mixed water region (Miyazawa et al. 2009; Masumoto et al. 2012). The processes are basically similar to those associated with the radionuclide dispersion reported by previous studies (e.g., Miyazawa et al. 2012, 2013). Relatively high concentrations of larger than 50 pg/l observed east of Japan during July and August 2011 are explained by the simulation (Fig. 5d, e). Figure 5d suggests that the concentration of two measurement points at 32.0°N–157.9°E and 35.9°N–165.0°E could be affected by the transport of the discharged PFOA along the Kuroshio Extension, although the simulation underestimates the absolute concentration levels. One year after the beginning of the simulation (Fig. 5f), the increased concentration almost disappears near Japan as a result of the eastward transport together with the horizontal and vertical mixing. Figure 5f also indicates that a low concentration smaller than 20 pg/l emerges around Japan, originating from the deeper layer; this will be discussed below.

Figure 6 shows that the high concentration reaches 100-m depth over a wide range east of Japan (Fig. 6a, b), while the high concentration is confined to areas near the coast at 200 m depth (Fig. 6c, d). The distributions of low concentrations smaller than 20 pg/l appear at 100 and 200 m depth near the Japanese coast in July and August 2011, and they are partially transported horizontally eastward along the Kuroshio Extension (Fig. 6c, d). The low concentration originates from the local upwelling associated with the horizontal shear of the Kuroshio in the shelf slope south of Japan (Kasai et al. 2002). The local upwelling is also shown in the Japan Sea and near the northern Kuril Islands (Fig. 6c, d).

Comparison of the simulated vertical profiles with the observed ones obtained near the east coast of Japan (Fig. 7a–c; also see Fig. 5e) indicates that the simulation represents concentrations larger than 50 pg/l at the upper 200-m depth as observed. The simulation represents sub-surface concentrations lower than the initial value in the upper 500 m, 23.3 pg/l, at a point around the Kuroshio Extension region (Fig. 7d), which is caused by the transport of low-concentration waters from the coastal area of Japan (Fig. 6c). The slight increase of the near-surface concentration shown in Fig. 7e, f resulted from the transport of the high-concentration waters along the Kuroshio Extension (Fig. 5d). The simulated profiles at two points (Fig. 7g, h) in the northern latitudes maintain the initial condition even 4 months after the beginning of the simulation, indicating that the simulated dispersion does not extend there (Fig. 5d).

The optimized parameter in the Green's function approach is represented by the summation of the contribution rates from each observation (see Eq. 12 in Miyazawa et al. 2013). Figure 8 shows the distributions of the contribution rate for the total emission amount (Fig. 8a), the initial concentration value in the upper 500-m water column (Fig. 8b), and the Smagorinsky diffusion constant (Fig. 8c). Measurement points over a wide range in the Western North Pacific, indicating a positive contribution rate of more than 1 % for the emission amount parameter (Fig. 8a), suggest that the accidental discharge of PFOA associated with EQ 3.11 actually affects the PFOA distribution in the Western North Pacific after a few months. Four points near the Japanese coast (three: 37.0°N–142.0°E, 38.0°N–143.5°E, 38.0°N–144.0°E) and far from there (one: 45.0°N–165.0°E) indicating a negative rate contribute to the reduced estimate of the optimized emission amount as compared to the first guess ('A-b-s' in Table 5). The measurement points sensitive to the initial value adjustment with the absolute values of a contribution rate larger than 20 % are distributed east of 155°E, far from
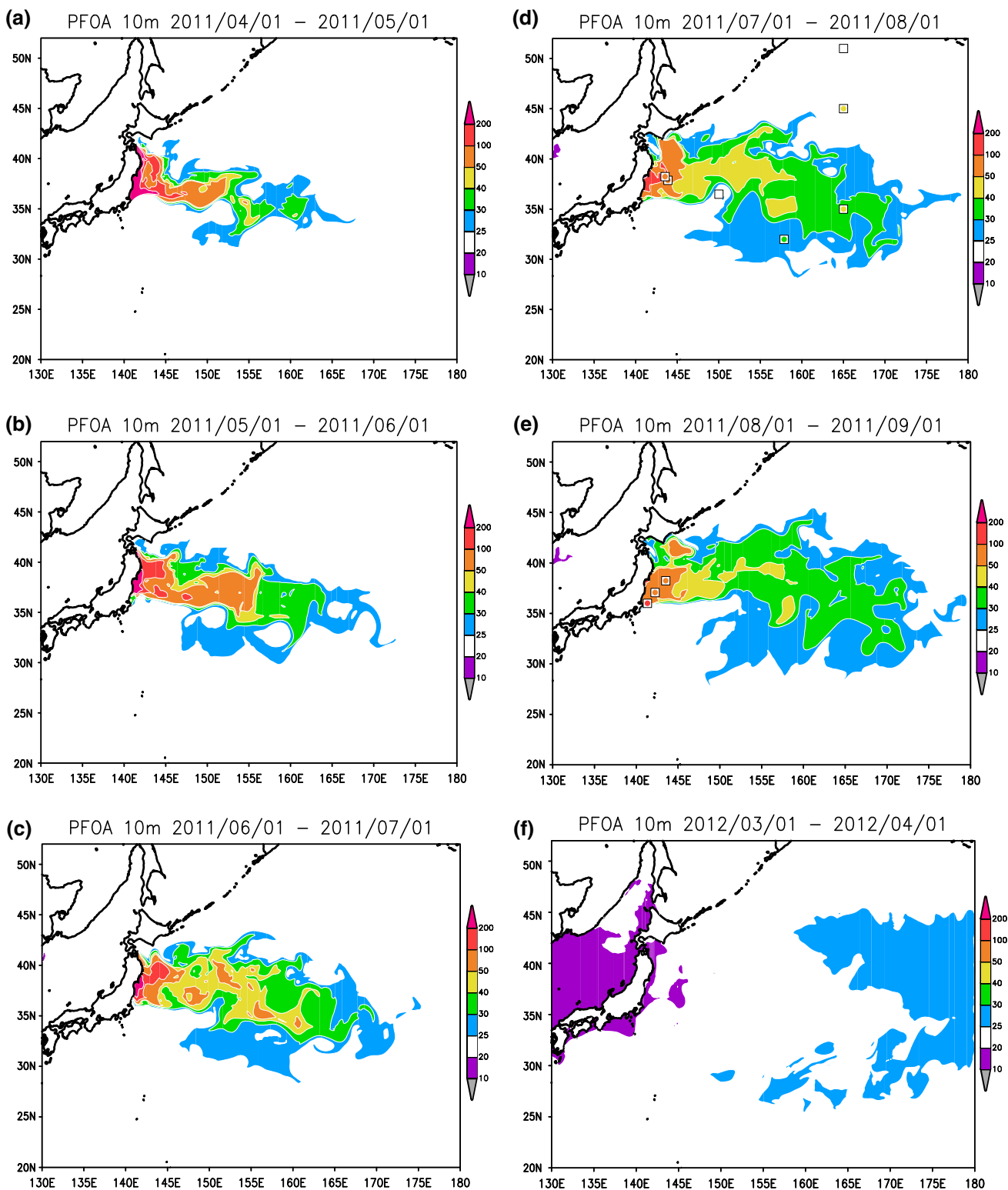
Fig. 5 Monthly mean distributions of the PFOA concentration (in pg/l) at 10 m depth represented by the simulation with the parameters optimized for the PFOA data ('PFOA-b-s' in Table 6). *Closed circles* in *squares* indicate the concentration measured in each month. *Color* *bars* of the *circles* are the same as those of the simulation. **a** April 2011, **b** May 2011, **c** June 2011, **d** July 2011, **e** August 2011, **f** March 2012
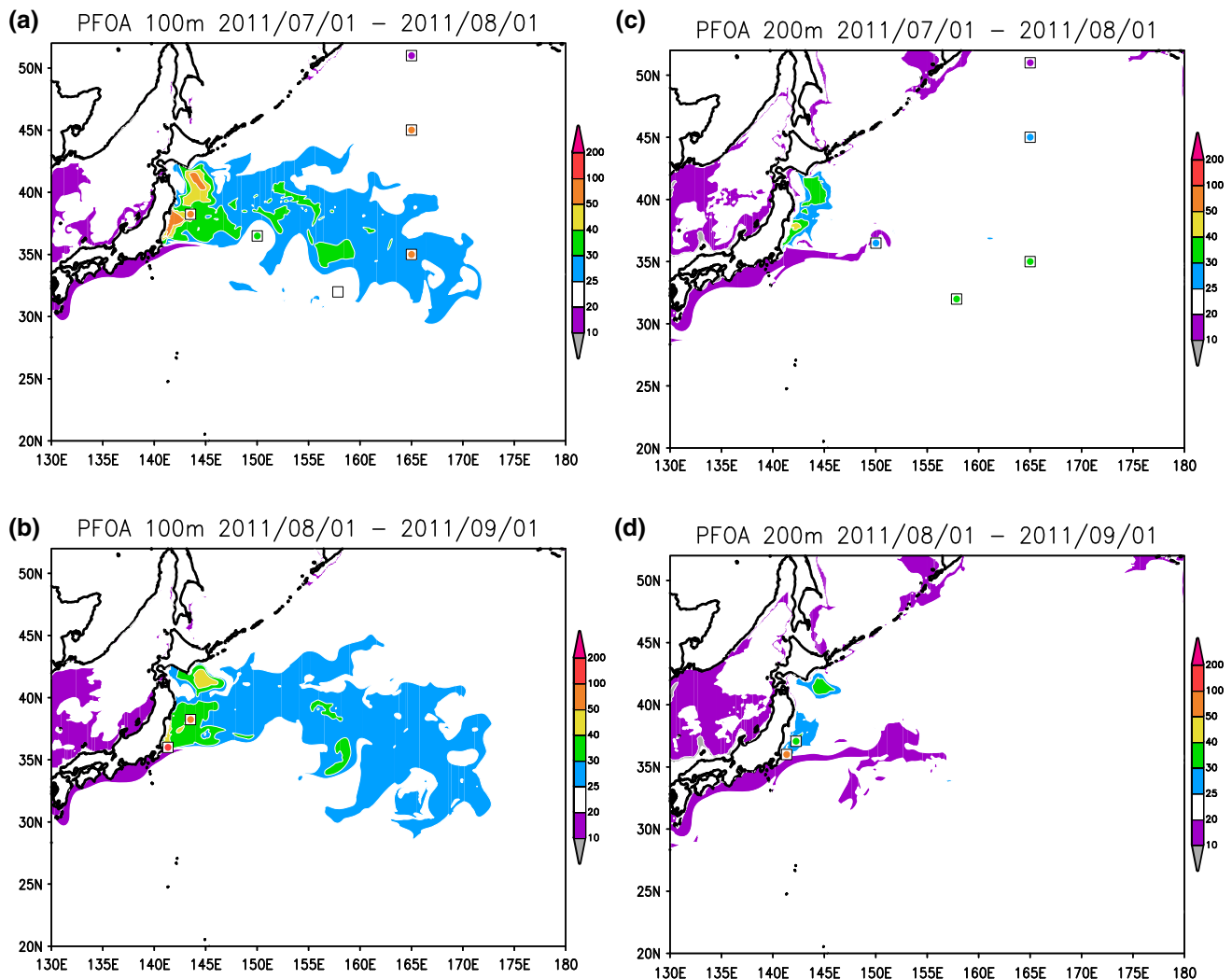
Fig. 6 As in Fig. 5, except at 100 m (**a, b**) and 200 m (**c, d**). **a, c** (**b, d**) denote the distributions in July (August) 2011

the source region (Fig. 8b), where the initial condition parameter works more effectively for the representation of the observed feature than the emission amount parameter. The increased estimation of the optimized diffusion parameter as compared to the first guess comes mainly from two measurement points (38.0°N–144.0°E and 36.5°N–150.0°E), while all other points indicate negative and/or small contribution rates within 20 % (Fig. 8c).

To check the effects of the surface data on the parameter optimization, we conduct the optimization with the addition of the surface observation data ('A-b-0', 'A-1-0', 'A-2-0', and 'A-3-0' in Table 5). The results interestingly indicate considerably reduced emission amounts and slightly increased initial values as compared to the results without the use of the surface data ('A-b-s', 'A-1-s', 'A-2-s', and 'A-3-s'). Longitudinal plots of both the observed and simulated PFOA concentration (Fig. 9) depict that the simulation represents a simple picture of the oceanic

dispersion originating from the source region: relatively higher concentrations in the subsurface layer and at the surface are confined near the coast west of 145°E. The subsurface observation generally represents similar features (Fig. 9a). In contrast, the surface observation data (Fig. 9b) are not consistent with the simple picture of oceanic dispersion, e.g., a relatively high concentration larger than 300 pg/l is found east of 155°E far from the source region. The correlation between the simulation and the observation becomes low if the observation includes the surface data (Table 7). The contribution rate distribution for the total emission amount in the optimization cases with the addition of the surface data (not shown) indicates almost negative values near the coast and negligible values smaller than 1 % far from the coast, suggesting that the direct discharge from the source region triggered by EQ 3.11 does not explain the observed surface concentration well. Note that use of the initial vertical profile with
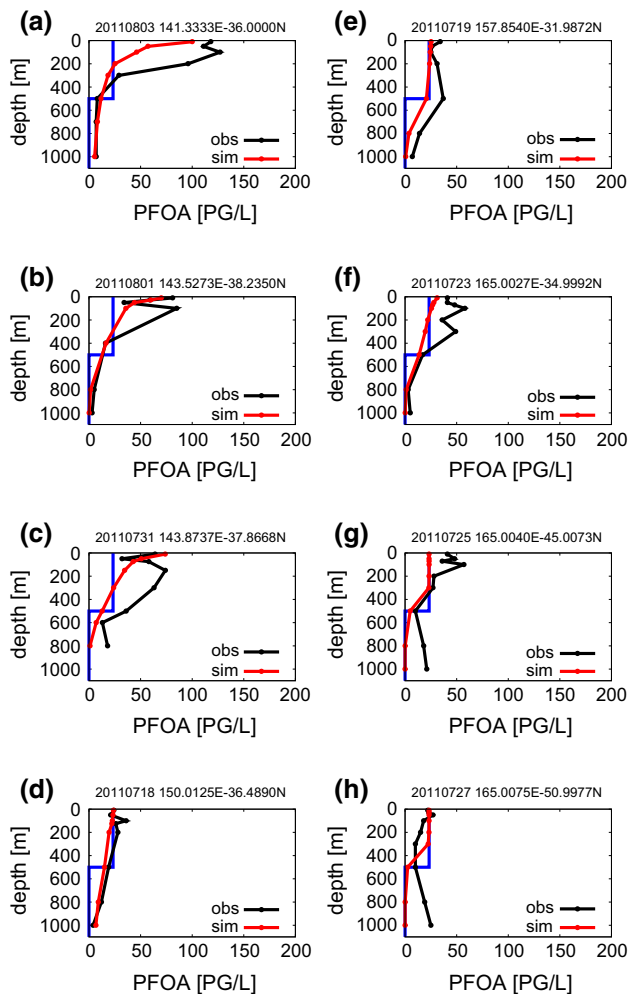
Fig. 7 Vertical profiles of the PFOA concentration. *Black* (*red*) curves denote the observation (the simulation with the parameters optimized for the PFOA data: 'PFOA-b-s' in Table 6). *Blue lines* denote the 'basic' initial profiles

the relatively high concentration at the surface (profile '3'), which implicitly represents the possible effect of the airborne PFAs, does not affect the parameter optimization results much.

3.2 The PFOS simulations

We conduct the parameter optimization using the PFOS observation data in the same manner as for the PFOA data (Table 6). The evaluated total emission amounts, initial values, and diffusion constants are smaller than those evaluated for the PFOA data in all cases. The evaluated smaller level of the PFOS concentration as compared with PFOA is consistent with previous studies (Yamashita et al. 2008). In contrast to the case of PFOA, the baseline simulation ('basic' in Table 1) shows poor capability to represent the observed PFOS data (Fig. 8a). Simulations with
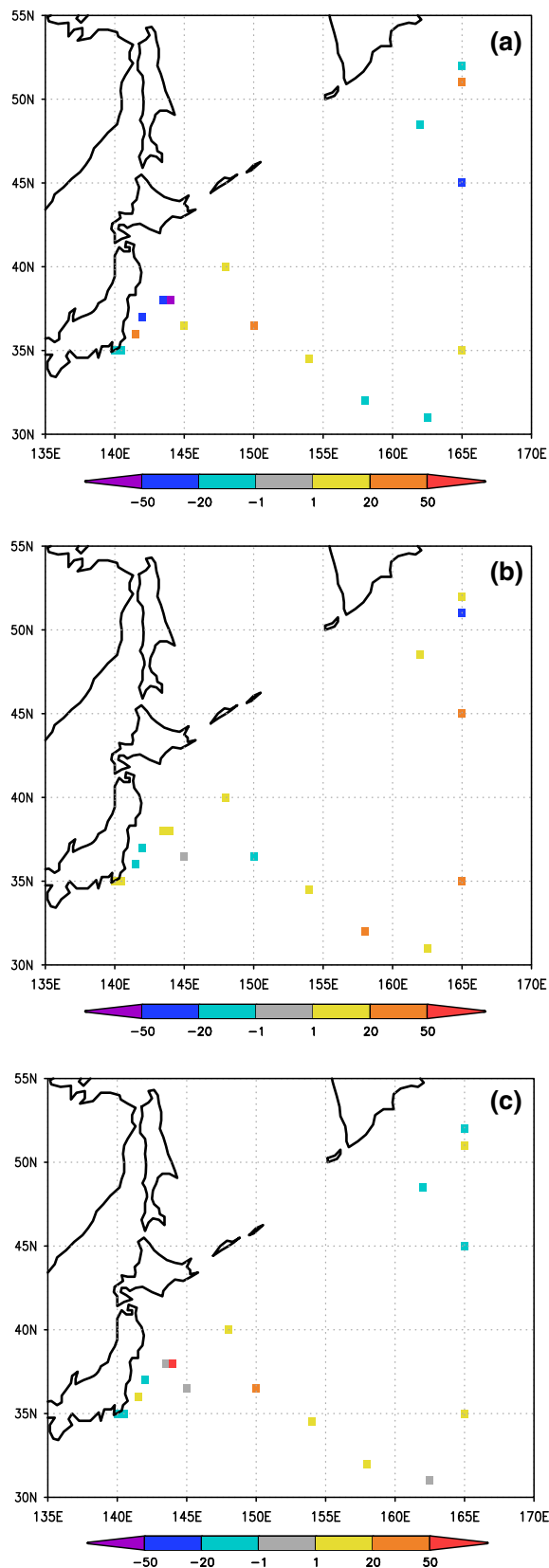

Fig. 8 Contribution rates (in %) averaged in 1/2° × 1/2° grids in the optimization case 'A-b-s'. **a** The total emission amount. **b** The initial value of the upper 500-m depth. **c** Smagorinsky diffusion constant

the optimized parameters result in correlation values smaller than the 95 % significance level of 0.22 (Table 7; also see Fig. 10b). Comparison between the simulated and observed PFOS profiles (Fig. 11) suggests that the simple assumptions about the accidental emission from the land and initial value confined in the upper layer are not valid
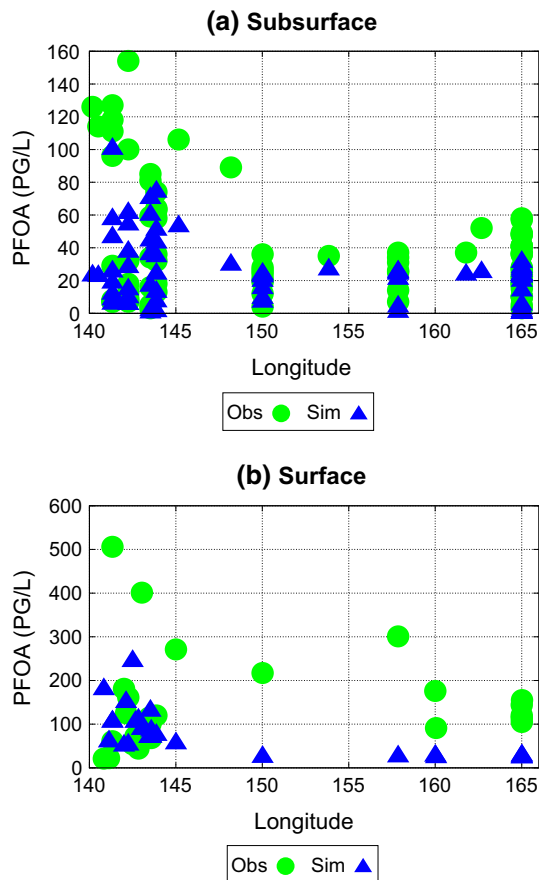

Fig. 9 Relations between the PFOA measurement longitudes and their concentration values. **a** Subsurface data. **b** Surface data. *Circles* (*triangles*) denote the data of the field observation (the simulation with the parameters optimized for the PFOA data: 'PFOA-b-s' in Table 6)

for the representation of the observed PFOS profiles. In particular, some of the observed profiles (Fig. 11a–c, f, h) represent two or three local subsurface maximums of the PFOS concentration, which seem not to be easily simulated by the relatively simple model adopted in the present study. Longitudinal plots of the PFOS observation data in the subsurface layer and at the surface (Fig. 12) exhibit a complicated feature that might not be simply explained by the present model (see also the correlation values for the data including the surface data described in Table 7).

4 Summary and discussion

Supposing an accidental emission of PFAs (PFOA and PFOS) into the ocean caused by the tremendous flood associated with the tsunami due to EQ 3.11, we performed a series of the numerical simulations representing the oceanic dispersion using an advection-diffusion model of the PFA concentration. The optimization of the parameters for the PFOA simulation—the total emission amount, initial concentration in the upper layer, and horizontal diffusion intensity—leads to improvement of the simulation skill representing the observed subsurface profiles of PFOA. The correlation coefficients between the observation and the simulations with the optimized parameters for the different types of initial vertical profiles result in a range of 0.60–0.63, and they generally succeed in representing the longitudinal contrast in the PFOA distribution that could be formed by the accidental emission.

Based on the results, we conclude that the present model's formulation is consistent with the real transport process of PFOA accidentally discharged into the ocean triggered by EQ 3.11, which could basically be described as the advection and diffusion processes related to the Kuroshio-Kuroshio Extension and the mesoscale eddies. Although the vertical entrainment of the low concentration water in the deep layer near the coasts seems to be a little bit exaggerated by the present setting of the initial

Table 6 Optimization results using the PFOS observation data

Cases (expected cost)	Initial profile	Use of surface data	Emission amount ± error (tons)	Initial value ± error	Diffusion constant ± error
S-b-s (1153)	Basic	No	0.8 ± 0.1	3.4 ± 0.2 (pg/l)	0.07 ± 0.03
S-1-s (1285)	1	No	1.8 ± 0.1	0.19 ± 0.02 (multiplication constant)	0.24 ± 0.03
S-2-s (1154)	2	No	1.0 ± 0.1	0.24 ± 0.01 (multiplication constant)	0.11 ± 0.02
S-3-s (1145)	3	No	1.0 ± 0.1	0.21 ± 0.01 (multiplication constant)	0.11 ± 0.02
S-b-0 (1660)	Basic	Yes	0.2 ± 0.04	4.0 ± 0.2 (pg/l)	0.09 ± 0.009
S-1-0 (1856)	1	Yes	0.3 ± 0.04	0.27 ± 0.01 (multiplication constant)	0.10 ± 0.009
S-2-0 (1637)	2	Yes	0.2 ± 0.04	0.30 ± 0.01 (multiplication constant)	0.09 ± 0.009
S-3-0 (1617)	3	Yes	0.1 ± 0.04	0.26 ± 0.01 (multiplication constant)	0.09 ± 0.009

Table 7 Parameters, cost, and correlation in the simulations with the parameters optimized for PFOA (A-b-s and A-2-s) and PFOS (S-b-s and S-2-s) data

| Cases	A-b-s simulation	A-2-s simulation	S-b-s simulation	S-2-s simulation
Total emission amount (tons)	4.8	5.0	0.8	1.0
Initial value	23 (pg/l)	1.8 (ratio)	3.4 (pg/l)	0.24 (ratio)
Diffusion constant	0.37	0.46	0.07	0.11
Cost function value for the PFOA data	614	619	–	–
Correlation with the PFOA data	0.60	0.63	–	–
Correlation with PFOA data including the surface data	0.34	0.37	–	–
Cost function value for the PFOS data	–	–	1,163	1,153
Correlation with the PFOS data	–	–	0.17	0.19
Correlation with PFOA data including the surface data	–	–	0.09	0.10
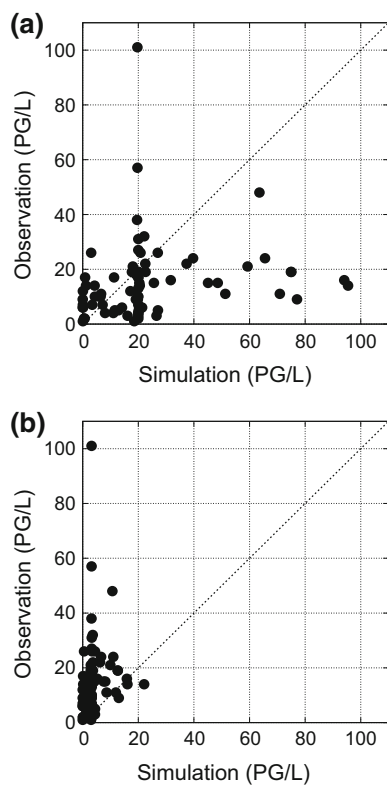
Fig. 10 Comparison of the observed and simulated PFOS concentration (in pg/l). **a** The baseline simulation ('basic' in Table 1). **b** The simulation with the parameters optimized for the PFOS data ('PFOS-b-s' in Table 6)

Fig. 11 As in Fig. 7 except for the PFOS observation and the simulation with the parameters optimized for the PFOS data ('PFOS-b-s' in Table 6)

condition with zero concentration below 500 m depth, the entrainment processes themselves are possible dynamical processes caused by the local upwelling associated with the cyclonic circulation in the frontal eddies of boundary currents (Lee et al. 1981) and/or the wind-driven coastal upwelling (Yoshida 1955).

Our simulation does not represent the PFOS distribution as observed well; the simulations with the parameters
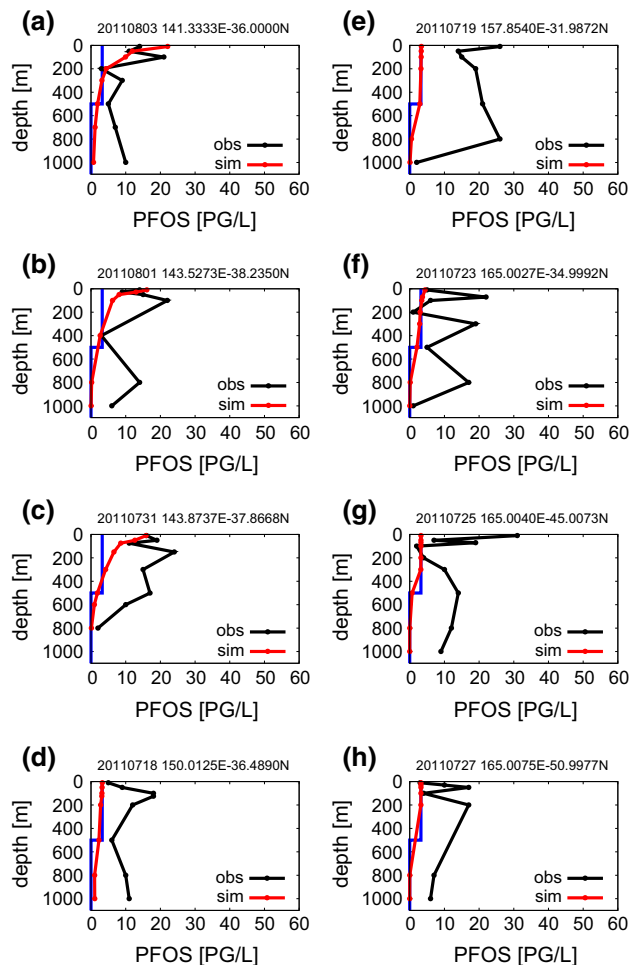
optimized for the PFOS observation data show a relatively low correlation, 0.17–0.19, as compared to the PFOA cases. The observed subsurface maxima of PFOS are poorly represented by the PFOS simulation (Fig. 11). The
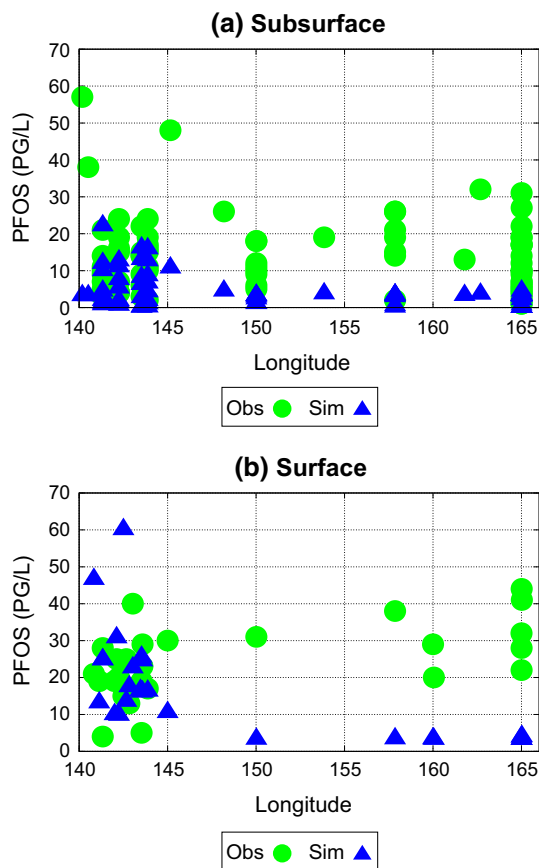
Fig. 12 As in Fig. 9 except for the PFOS data. *Triangles* denote the data of the simulation with the parameters optimized for the PFOS data: 'PFOS-b-s' in Table 6

PFOA simulation also fails to represent the subsurface maximum around 100–200 m depth (Fig. 7a–c). Comparison of the observed PFOA and PFOS profiles suggests that PFOS seems to penetrate deeper than PFOA. Those results suggest that our assumptions of modeling the emission and transport are not completely appropriate for description of the actual oceanic transport processes of PFAs. The difference between the capabilites of PFOA and PFOS simulations might be related to the fact that PFOS is not very soluble in water and is more bio-accumulative as compared to PFOA (Nakata et al. 2006). More complicated processes including the sediment dynamics and biological effects should be included in the transport model of PFAs and could be investigated by future studies.

Our modeling of the oceanic transport of PFA involves the uncertainty of the initial condition. The parameter optimization for the different types of initial vertical profiles causes a difference in the evaluation of the total emission amounts: 4.8–6.7 (tons) for PFOA and 0.8–1.8 (tons) for PFOS. We note that the initial profile types representing higher concentrations near the surface ('basic', '2', and '3'), which are similar to the typical

profiles around industrial countries such as Japan (Yamashita et al. 2005, 2008), clearly exhibit smaller cost estimates as compared to the case with an initial profile with a subsurface maximum concentration ('1'). The total emission estimates excluding the case with the profile '1' show narrower ranges of the estimates: 4.8–5.1 (tons) for PFOA and 0.8–1.0 (tons) for PFOS.

Note that all simulations with different initial vertical profiles fail to represent the observed subsurface maxima of both the PFOA and PFOS observation data (e.g., Fig. 7, 11). These seem to be pre-existing states and could not be from the EQ 3.11-related signals, especially for PFOS, although the missing mechanisms also could be responsible for the poor capability of representing the subsurface maxima, as mentioned above. The available observation data on PFAs are still few and not enough to even create a climatological view of the horizontal and vertical distributions. For a more accurate description of PFAs' oceanic variability, we need to clarify the climatological view of the horizontal and vertical distribution by accumulating more observation data and/or by performing the simulations designed for representation of the climatological states.

The optimization results depend on the prescription of the observation error of PFAs. The present study assumes that the observation error is given by 20 % of the measurement value. In such cases, the optimization tends to underestimate the comparatively high concentration of the observed PFOA because the observation data for higher concentrations and larger observation errors are less weighted for the cost function than those with lower concentrations and smaller errors. Assuming a constant 1 pg/l of the observation error for all PFOA data, the optimization results in a smaller emission amount: 4.4 ± 0.06 tons, a larger initial value, 46 ± 0.2 pg/l, and a smaller Smagorinsky diffusion constant, 0.18 ± 0.01. Interestingly, the estimate of the emission amount is not affected much by the error prescription as compared to that of the initial value parameter.

The addition of the surface observation data to the cost function considerably affects the parameter optimization. A simple emission process assuming the accidental input of PFAs into the ocean alone is not enough to represent the complicated surface distribution. Figures 9b and 12b suggest that the observed PFOA (PFOS) concentration distribution at the surface has O (100 pg/l) (O (10 pg/l)) variability range over the Western North Pacific, which is possibly caused by the airborne PFOA (PFOS). Surface boundary conditions representing the supply of the airborne PFAs into the ocean besides the condition of no flux at the surface adopted in the present model might be required for improvement of the capability to reproduce the surface distribution.

References

Furuichi N, Hibiya T, Niwa Y (2012) Assessment of turbulence closure models for resonant inertial response in the oceanic mixed layer using a large eddy simulation model. J Oceanogr 68:285–294

Giesy JP, Kannan K (2001) Global distribution of perfluorooctane sulfonate in wildlife. Environ Sci Technol 35:1339–1342

Kasai A, Kimura S, Nakata H, Okazaki Y (2002) Entrainment of coastal water into a frontal eddy of the Kuroshio and its biological significance. J Mar Sys 37:185–198

Lee TN, Atkinson LP, Legeckis R (1981) Observation of a Gulf Stream frontal eddy on the Georgia continent shelf, April 1977. Deep Sea Res 28A:347–378

Masumoto Y, Miyazawa Y, Tsumune D, Kobayashi T, Estournel C, Marsaleix P, Lanerolle L, Mehra A, Garraffo ZD (2012) Oceanic dispersion simulation of cesium 137 from Fukushima Daiichi Nuclear Power Plant. Elements 8:207–212

Mellor G (2004) Users guide for a three-dimensional, primitive equation, numerical ocean model. J Phys Oceanogr 34(3):693–698

Menemenlis D, Fukumori I, Lee L (2005) Using Green's functions to calibrate an ocean general circulation model. Mon Wea Rev 133:1224–1240

Miyazawa Y, Zhang RC, Guo X, Tamura H, Ambe D, Lee JS, Okuno A, Yoshinari H, Setou T, Komatsu K (2009) Water mass variability in the western North Pacific detected in a 15 year eddy resolving ocean reanalysis. J Oceanogr 65(6):737–756

Miyazawa Y, Masumoto Y, Varlamov SM, Miyama T (2012) Transport simulation of the radionuclide from the shelf to open ocean around Fukushima. Cont Shelf Res 50–51:16–29

Miyazawa Y, Masumoto Y, Varlamov SM, Miyama T, Takigawa M, Honda M, Saino T (2013) Inverse estimation of source parameters of oceanic radioactivity dispersion models associated with the Fukushima accident. Biogeosciences 10:2349–2363

Nakajima H, Koarai M (2011) Assessment of tsunami flood situation from the Great East Japan earthquake. Bull Geospat Inf Auth Jpn 59:55–66

Nakanishi M, Niino H (2009) Development of an improved turbulence closure model for the atmospheric boundary layer. J Meteorol Soc Jpn 87:895–912

Nakata H, Kannan K, Nasu T, Cho H-S, Sinclair E, Takemura A (2006) Perfluorinated contaminants in sediments and aquatic organisms collected from shallow water and tidal flat areas of the Ariake Sea, Japan: environmental fate of perfluorooctane sulfonate in aquatic ecosystems. Env Sci Tech 40:4916–4921

Showstack R (2011) Oceanographer tracks marine debris from the Japan tsunami and other incidents. EOS Trans AGU 92(37):306

Smagorinsky J (1963) General circulation experiments with the primitive equations. I. The basic experiment. Mon Wea Rev 91:99–164

Yamashita N, Kannan K, Taniyasu S, Horii Y, Okazawa T, Petrick G, Gamo T (2004) Analysis of perfluorinated acids at partsper-quadrillion levels in seawater using liquid chromatography-tandem mass spectrometry. Environ Sci Technol 38:5522–5528

Yamashita N, Kannan K, Taniyasu S, Horii Y, Petrick G, Gamo T (2005) A global survey of perfluorinated acids in oceans. Mar Pollut Bull 51:658–668

Yamashita N, Taniyasu S, Petrick G, Wei S, Gamo T, Lam PKS, Kannan K (2008) Perfluorinated acids as novel chemical tracers of global circulation of ocean waters. Chemosphere 70:1247–1255

Yamazaki E, Yamashita N, Taniyasu S, Petrick G, Tanhua T, Kannan K, Gamo T (2012) Accidental input of perfluoroalkyl substances from land to ocean by the disaster of tsunami, EQ3.11, Japan. Organohalog Compd 74(B1B):103

Yoshida K (1955) Coastal upwelling off the California coast. Rec Oceanogr Wks Japan New Ser 2:8–20